THE JOURNAL OF PHYSICAL CHEMISTRY C

Article

pubs.acs.org/JPCC

Investigation of the Redox Chemistry of Isoindole-4,7-diones

Christoffer Karlsson,[†] Adolf Gogoll,[‡] Maria Strømme,[†] and Martin Sjödin*[,†]

[†]Nanotechnology and Functional Materials, Department of Engineering Sciences, The Ångström Laboratory, Uppsala University, Box 534, SE-751 21 Uppsala, Sweden

[‡]Department of Chemistry - BMC, Biomedical Centre, Uppsala University, Box 576, SE-751 23 Uppsala, Sweden

Supporting Information

ABSTRACT: Quinone derivatives have been proposed as active components in lithium ion battery (LIB) electrode materials. In this work the electrochemistry of a series of substituted isoindole-4,7-diones (IIDs) was investigated. Three new IID derivatives were synthesized and characterized by various electrochemical and spectroscopic techniques. Polymerization was attempted to achieve a conducting polymer with redox active quinone side groups, which would be advantageous in a LIB application. A combination of *in situ* spectroelectrochemical measurements and density functional theory (DFT) calculations was used to investigate the proton coupled redox reactions of the IIDs. Results from a previous computational study of the IIDs were compared with experimental data here, and the agreement was very good. The energy of the spectroscopic transitions in the UV and in the visible region showed different correlation with redox potential and quinone substituent in the series of IIDs. This behavior was rationalized by examination of the involved molecular orbitals. The results indicated that the properties of the quinone unit, such as the redox potential, could be selectively varied by substitution.

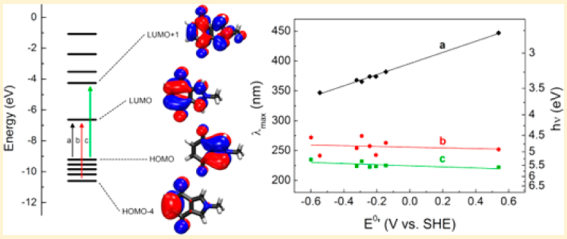

1. INTRODUCTION

Inorganic Li intercalation compounds, such as $LiCoO_2$, are currently used in commercially available lithium ion battery (LIB) cathodes. Those materials are expensive to produce due to the large amounts of energy required to refine them, which also makes recycling relatively expensive.[1] Development of redox active organic molecules that can replace the inorganic LIB materials has therefore gained large interest.[1−3] Several *p*-benzoquinone derivatives have been proposed as active components in LIB electrode materials.[4,5] Such organic matter based cathodes are expected to be cheaper, more environmentally friendly, and have higher specific energies and higher specific capacities than inorganic lithium intercalation compounds. They could also reduce problems with swelling upon cycling, since they are amorphous.[6]

We have previously suggested isoindole-4,7-dione (IID) derivatives as a new group of candidate materials for organic LIB cathodes,[7] with a theoretical capacity of up to 333 mAh/g (for the reduced dilithium form of IID). IID contains a redox active *p*-benzoquinone group as well as a pyrrole moiety that could allow for polymerization.[8,9] Problems with degradation due to dissolution, which are usually encountered for small organic molecules when used as active battery material, could be resolved by polymerization of IID.[4,10] In addition, the resulting polymer would be conductive, decreasing resistance in the material and possibly eliminating the need for conductive additives. Ideally, an IID polymer would have the well-defined redox potential of the quinone moieties[4,7] and also the capacitive charging of the conductive polypyrrole backbone.[11,12]

The properties of the quinone redox system have been extensively studied both experimentally[13,14] and computationally.[15−17] Indeed, computations provide useful tools for predicting key parameters, such as redox potentials, specific energies, and pK_a values. However, due to the existence of a radical semiquinone state and the possibility of proton transfers involved in all redox reactions, quinones exhibit quite complex electrochemistry.[13] This makes prediction of quinone electrochemistry difficult, and many studies simplify the calculations by not considering all possible forms of oxidation and protonation.[15,16]

In this work we continue our investigation of the proton coupled IID redox system.[7] The series of IID derivatives has been extended by three new synthesized compounds to achieve a better understanding of the influence of substitution on the redox chemistry. The design principles and the computational strategy used in the survey of IIDs can be employed for any redox active monomer, and they are especially useful when protonation reactions are involved. It is thus a useful tool for understanding the redox chemistry of complex quinone systems.

2. EXPERIMENTAL AND THEORETICAL METHODS

5,8-Dihydroxy-1,4-naphthoquinone was purchased from Atomole Scientific; other reagents were purchased from Sigma-Aldrich. All reagents were used without further purification.

Received: November 7, 2012
Revised: December 18, 2012
Published: December 18, 2012

Flash chromatography was performed using VWR Normasil 60 silica gel (40−63 μm, 60 Å). NMR spectra were recorded on a Varian INOVA (^{1}H at 499.93 MHz, ^{13}C at 125.71 MHz) or a Varian UNITY (^{1}H at 399.97 MHz, ^{13}C at 100.58 MHz) spectrometer. Chemical shifts are reported using the chloroform solvent signal as an indirect reference to TMS (δ_H = 7.26 ppm, δ_C = 77.00 ppm). NMR signals were assigned from HSQC and HMBC spectra. IR ATR spectra were recorded on a PerkinElmer Spectrum One spectrophotometer. ESI mass spectra were recorded on a Finnigan Thermoquest AQA mass spectrometer. Melting points were measured with a Stuart Scientific SMP10. UV/vis spectra were recorded on an Agilent 8453 UV−vis spectrophotometer using a quartz cuvette with 1 mm path length.

2.1. Electrochemistry. An Autolab PGSTAT302N potentiostat (Ecochemie, The Netherlands) was used for all electrochemical measurements. The analyte concentration was 1.0 mM in ∼5 mL of either organic or aqueous electrolyte. The organic electrolyte used was 0.1 M tetrabutylammonium hexafluorophosphate (TBAHFP) in acetonitrile (MeCN). The aqueous electrolyte consisted of 1 M $NaNO_3$ buffered with phosphate, borate, and acetate ions (10 mM each), and the pH was tuned with HNO_3(aq). In some cases, this analyte solution was mixed with EtOH (1:1 v/v) to increase solubility of the analyte. All potentials measured in aqueous solutions are reported versus the standard hydrogen electrode (SHE), and all potentials measured in organic solutions are reported versus the ferrocene couple (Fc^0/Fc^+), unless otherwise specified. A polished and sonicated glassy carbon disk electrode (3.0 mm diameter) was used as working electrode, and a Pt wire was used as counter electrode. The reference electrode was kept in a separate compartment and consisted of a Ag/AgCl electrode (3 M NaCl, 0.197 V vs SHE) in aqueous solutions and a Ag^0/Ag^+ electrode (10 mM $AgNO_3$, 0.1 M TBAHFP, −0.096 V vs Fc^0/Fc^+) in MeCN solutions. Analyte solutions were thoroughly degassed with N_2(g) and kept under a N_2(g) atmosphere throughout the measurements. Spectroelectrochemical measurements were performed in ∼200 μL of organic electrolyte with an analyte concentration of 1.0 mM, using a quartz cuvette with 1 mm path length as a thin layer cell with a Pt gauze as the working electrode. The counter electrode was kept in a separate compartment, and the reference electrode was immersed directly into the analyte solution.

2.2. General Synthesis Procedure. The IIDs **1**−**4** were synthesized according to a previously published procedure of **1** (Scheme 1).[7] Substituted *p*-benzoquinone (2.0 mmol), sarcosine (4.0 mmol, 356 mg), and paraformaldehyde (10 mmol, 300 mg) were dissolved in toluene (20 mL). The reaction mixture was refluxed for 1 h using a Dean−Stark apparatus. The solvent was evaporated, and the crude residue was purified with flash chromatography (EtOAc/pentane gradient, 1:4−1:1). The product was obtained after evaporation of solvent. IR and NMR spectra for all compounds are available in Figures S1−S12.

Scheme 1. Synthesis of IIDs[a]

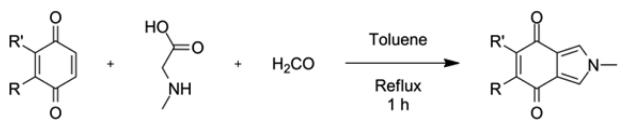

[a] **1**: R = R′ = H; **2**: R = Cl, R′ = H; **3**: R = *t*Bu, R′ = H; **4**: R−R′ = −COH=CH−CH=COH−.

*2-Methylisoindole-4,7-dione (**1**).* *p*-Benzoquinone (216 mg) was used as starting material. Yellow crystals; 48 mg (15% isolated yield); mp = 207 °C. ^{1}H NMR ($CDCl_3$, 400 MHz): δ_H = 7.20 (s, 2H, H-1, H-3), 6.64 (s, 2H, H-5, H-6), 3.77 (s, 3H, CH_3) ppm. ^{13}C NMR ($CDCl_3$, 100 MHz): δ_C = 182.0 (C=O), 139.7 (C-5, C-6), 124.6 (C-1, C-3), 121.7 (C-3a, C-7a), 37.2 (CH_3) ppm. IR (neat): 3132 (CH), 3071 (CH), 2953 (CH_3), 2924 (CH_3), 2853 (CH_3), 1649 (C=O), 1640 (C=O) cm^{-1}. UV/vis (MeCN): λ_{max} = 225, 242, 369 nm. MS (ESI) *m*/*z* = 162 ([M + H]$^+$), 163 ([M + 2H]$^+$), 164 ([M + 3H]$^+$), 203 ([M + MeCN + H]$^+$).

*5-Chloro-2-methylisoindole-4,7-dione (**2**).* Chloro-*p*-benzoquinone (216 mg) was used as starting material. Yellow crystals; 27 mg (9% isolated yield); mp >300 °C; **1** was also formed in the reaction, 16 mg (7% isolated yield). ^{1}H NMR ($CDCl_3$, 500 MHz): δ_H = 7.31 (d, *J* = 1.7 Hz, 1H, H-3), 7.21 (d, *J* = 1.7 Hz, 1H, H-1), 6.93 (s, 1H, H-6), 3.79 (s, 3H, CH_3) ppm. ^{13}C NMR ($CDCl_3$, 100 MHz): δ_C = 179.5 (C-7), 174.0 (C-4), 147.1 (C-5), 136.7 (C-6), 126.4 (C-3), 125.0 (C-1), 122.0 (C-7a), 120.7 (C-3a), 37.4 (CH_3) ppm. IR (neat): 3117 (CH), 3075 (CH), 2956 (CH_3), 2924 (CH_3), 2854 (CH_3), 1660 (C=O), 1642 (C=O) cm^{-1}. UV/vis (MeCN): λ_{max} = 225, 263, 382 nm. MS (ESI) *m*/*z* = 145 ([M−Cl−CH_3]$^+$), 152 ([M−CO−CH_3]$^+$), 154 ([M−$CHNCH_3$]$^+$), 164 ([M−2O]$^+$), 166 ([M−NCH_3]$^+$), 195 (M$^+$).

*5-tert-Butyl-2-methylisoindole-4,7-dione (**3**).* *tert*-Butyl-*p*-benzoquinone (328 mg) was used as starting material. Yellow crystals; 156 mg (36% isolated yield); mp = 175 °C. ^{1}H NMR ($CDCl_3$, 500 MHz): δ_H = 7.15 (d, *J* = 1.7 Hz, 1H, H-3), 7.13 (d, *J* = 1.7 Hz, 1H, H-1), 6.54 (s, 1H, H-6), 3.75 (s, 3H, NCH_3), 1.32 (s, 9H, $C(CH_3)_3$) ppm. ^{13}C NMR ($CDCl_3$, 100 MHz): δ_C = 182.9 (C-7), 182.1 (C-4), 158.7 (C-5), 135.0 (C-6), 125.1 (C-3), 123.8 (C-3a), 123.4 (C-1), 121.6 (C-7a), 37.2 (NCH_3), 35.6 ($\underline{C}(CH_3)_3$), 29.6 ($C(\underline{C}H_3)_3$) ppm. IR (neat): 3120 (CH), 3079 (CH), 3055 (CH_3^{tBu}), 3007 (CH_3^{tBu}), 2965 (CH_3^{tBu}), 2957 (CH_3^{NMe}), 2926 (CH_3^{NMe}), 2912 (CH_3^{NMe}), 1658 (C=O), 1645 (C=O) cm^{-1}. UV/vis (MeCN): λ_{max} = 224, 254, 368 nm. MS (ESI) *m*/*z* = 190 ([M + H−CO]$^+$), 218 ([M + H]$^+$), 259 ([M + MeCN]$^+$).

*5,8-Dihydroxy-2-methylbenzo[f]isoindole-4,9-dione (**4**).* 5,8-Dihydroxy-1,4-naphthoquinone (380 mg) was used as starting material. Red crystals; 78 mg (16% isolated yield); mp = 282 °C. ^{1}H NMR ($CDCl_3$, 500 MHz): δ_H = 7.39 (s, 2H, H-1, H-3), 7.18 (s, 2H, H-6, H-7), 3.85 (s, 3H, CH_3) ppm. ^{13}C NMR ($CDCl_3$, 100 MHz): δ_C = 184.9 (C=O), 157.6 (C-5, C-8), 128.4 (C-6, C-7), 125.5 (C-1, C-3), 122.7 (C-3a, C-9a), 114.4 (C-4a, C-8a), 37.6 (CH_3) ppm. IR (neat): 3125 (CH), 3077 (CH), 2954 (CH_3), 2919 (CH_3), 2851 (CH_3), 1646 (C=O) cm^{-1}. UV/vis (MeCN): λ_{max} = 235, 272, 281, 341, 357, 384, 423, 436, 447, 460, 474, 489 nm. MS (ESI) *m*/*z* = 190 ([M + H−C_2H_2OH]$^+$), 218 ([M + H−C_2H_2]$^+$), 244 ([M + H]$^+$).

2.3. Density Functional Theory Calculations. All density functional theory (DFT) calculations were performed at the B3LYP level of theory with the 6-311+G(d) basis set, using Gaussian 09.[18] Results from a previous study,[7] in which the same method was used, are compared with experimental data here. Molecular structures were optimized in the gas phase, and time-dependent (TD-SCF) energy calculations were performed on the optimized structures to calculate the energies of the excited states in MeCN solution, using the PCM solvation

dx.doi.org/10.1021/jp311009z | J. Phys. Chem. C 2013, 117, 894−901

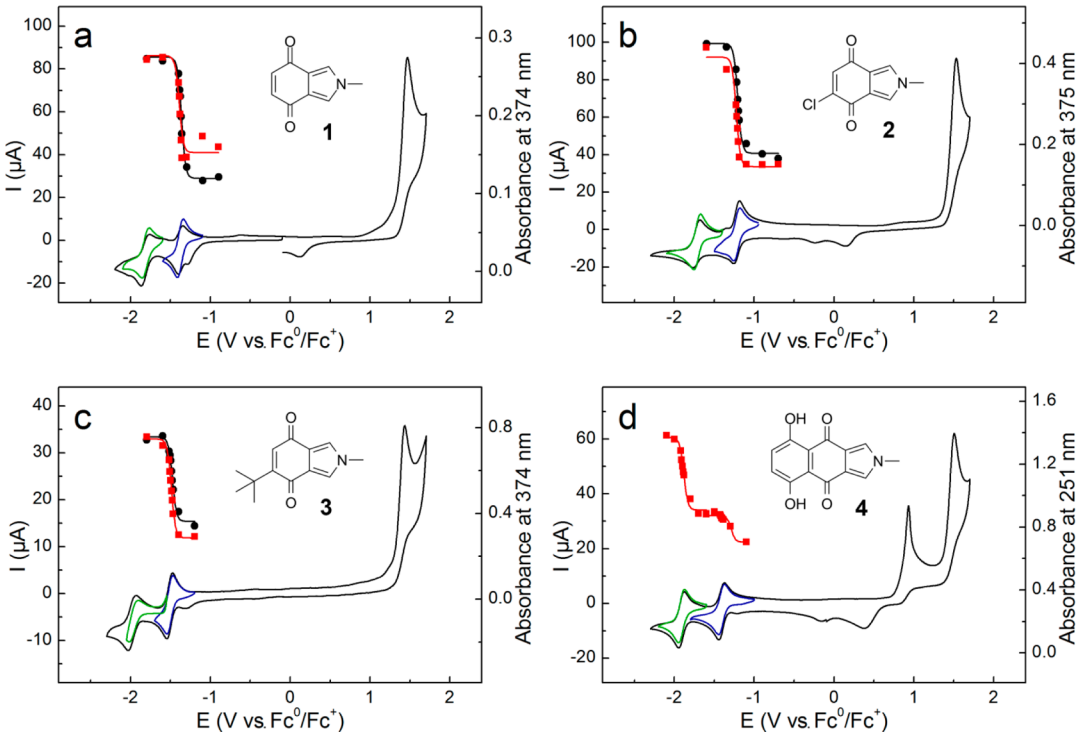

Figure 1. CVs of (a) **1**, (b) **2**,[27] (c) **3**, and (d) **4** in MeCN (0.1 V/s, second scan, black line) with sweeps over each reversible redox peak, corresponding to the Q/SQ (blue line) and SQ/HQ (green line) transition. At high potentials, the irreversible oxidation to the pyrrole centered cation radical can be seen. In panel d, there is also a two-electron oxidation to **5**. The UV/vis absorbance at a peak maximum during potentiostatic reduction (red squares) and oxidation (black circles) is overlaid, with fits to the Nernst equation (solid lines).

Table 1. Diffusion Coefficients, Peak Splits, and Difference between Peak Potentials and Potentials at Half-Peak Height of the Reduction (Red) and Oxidation (Ox) Peaks in CV at 0.1 V/s in MeCN

	D (10^{-6} cm^2/s)			ΔE_p (mV)		$E_p - E_{p/2}$ (mV)			
no.	Q	SQ	HQ	HQ/SQ	SQ/Q	Red HQ/SQ	Red SQ/Q	Ox HQ/SQ	Ox SQ/Q
1	8.1	6.5	3.7	77	69	60	58	61	54
2	10.3	9.5	6.4	73	67	63	65	63	54
3	1.2	1.4	0.31	91	71	69	60	71	60
4	2.0	1.7	3.3	69	69	58	54	58	60

Table 2. Calculated[7] and Experimentally Determined Redox Potentials of 1−5 in Neutral Aqueous Solution (V vs SHE) and in MeCN (V vs Fc^0/Fc^+, Experimentally Determined)

			$E^{0\prime}$ (aq, pH = 7)		E^0 (MeCN)		
no.	R	R′	calcd	exptl	HQ/SQ	SQ/Q	$Q/Q^{\bullet+}$ [a]
1	H	H	−0.209	−0.205	−1.803	−1.375	1.415
2	Cl	H	−0.188	−0.145	−1.691	−1.214	1.478
3	*t*Bu	H	−0.294	−0.322[b]	−1.935	−1.499	1.387
4	−COH=CH−CH=COH−		−0.738	−0.599[b]	−1.906	−1.408	
5	−CO−CH=CH−CO−		0.585	0.539[b]	0.895[c]		1.460

[a]Maximum slope of the irreversible oxidation peak. [b]The electrolyte was 1 M $NaNO_3$(aq)/EtOH (1:1 v/v), with buffer ions. [c]Maximum slope of the two-electron oxidation from **4**.

model with the UAKS topological model. Molecular orbitals (MOs) were constructed using the 6-311G basis set and were visualized with VMD.[19]

3. RESULTS

3.1. Electrochemistry. The redox behavior of **2**−**4** was investigated by square wave voltammetry (SWV), differential pulse voltammetry (DPV), and cyclic voltammetry (CV). In organic media, all compounds could be reduced in two reversible one-electron steps from the quinone (Q) to the respective semiquinone (SQ) and hydroquinone (HQ) species (Figure 1). At high potentials, they could also be irreversibly oxidized to the pyrrole centered cation radical.[7] Additionally, **4** showed a nonreversible oxidation peak at 0.895 V vs Fc^0/Fc^+, corresponding to the conversion to 2-methylbenzo[*f*]isoindole-4,5,8,9-tetraone (**5**). The current could be fully recovered, but the shape of the voltammogram indicated a more complicated redox reaction, possibly involving adsorption of **5** to the

dx.doi.org/10.1021/jp311009z | J. Phys. Chem. C 2013, 117, 894−901

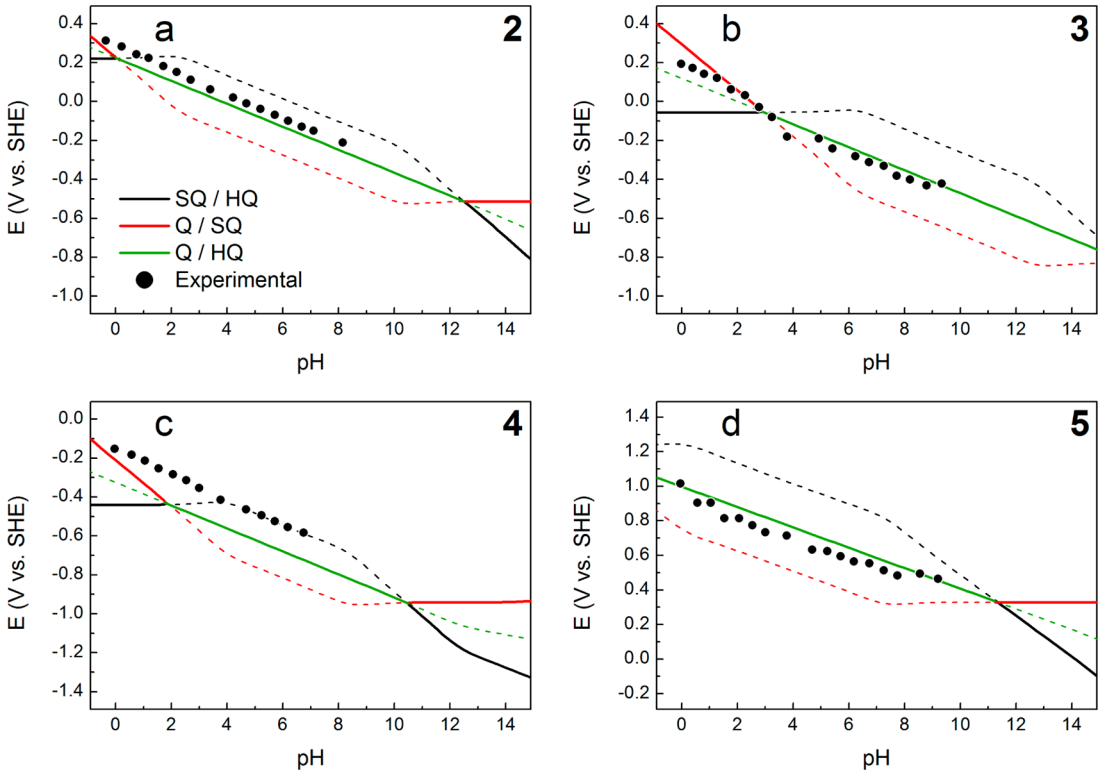

Figure 2. Pourbaix diagrams with calculated and experimental redox potentials for (a) **2**, (b) **3**, (c) **4**, and (d) **5** in buffered aqueous solution. Lines show calculated redox potentials for the SQ/HQ (black), Q/SQ (red), and Q/HQ (green) reactions. The expected observable redox reactions are indicated by thick solid lines. Experimental redox potentials determined by DPV reduction potentials are overlaid (black circles).

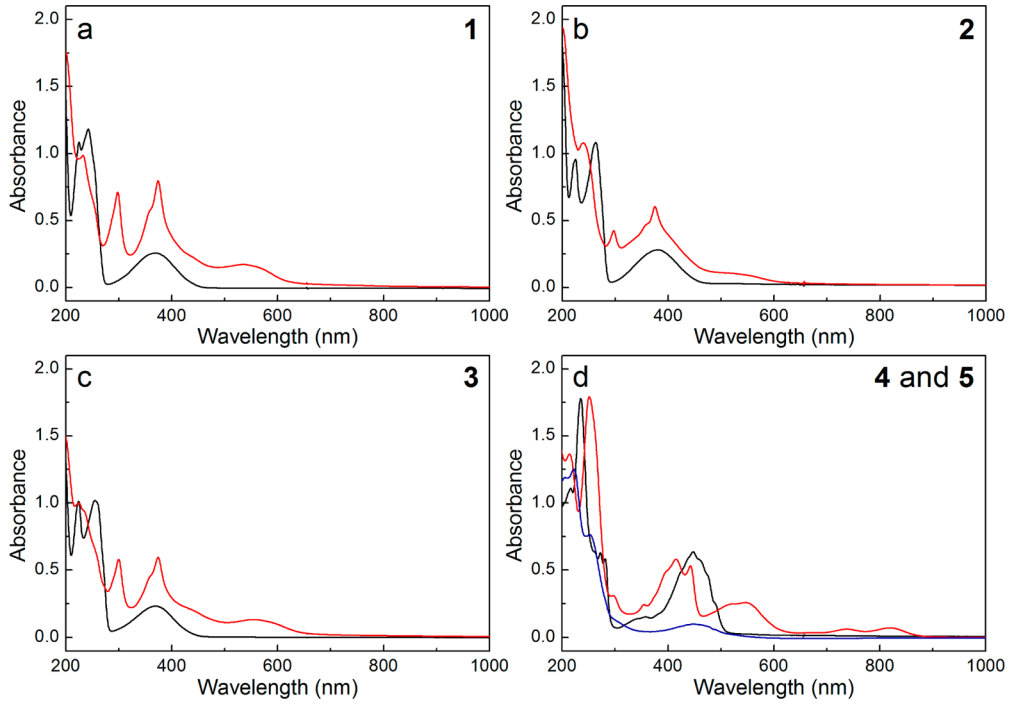

Figure 3. UV/vis spectra of (a) **1**, (b) **2**, (c) **3**, and (d) **4** in the oxidized (black, Q) and reduced (red, SQ) state, after *in situ* potential step oxidation/reduction. The spectrum of **5** is also included in panel d (blue), obtained after oxidation of **4**.

electrode surface. The peak currents for the reversible redox reactions were found to be linearly dependent on the square root of the scan rate and diffusion coefficients of the Q, SQ, and HQ species of **1**–**4** were determined from the scan rate dependency data (Table 1). E^0 values in MeCN were calculated as the average of the reduction and oxidation peak potentials (Table 2). In buffered aqueous solution, a nonreversible redox reaction, corresponding to the two-electron redox interconversion of the Q and HQ species, was observed (with peak splits ranging from 60 mV to 1.2 V). The formal potential for this

dx.doi.org/10.1021/jp311009z | *J. Phys. Chem. C* 2013, 117, 894–901

reaction was highly pH-dependent for all IIDs investigated in this study in the pH range between 0 and 10 (Figure 2). The pH dependence of the formal potential was previously published for **1**,[7] and the electrochemical behavior of **2**−**4** is analogous. DPV reduction peak potentials were used to evaluate $E^{0\prime}$ values in aqueous solution (Table 2).

3.2. Spectroelectrochemistry. **1**−**4** were reversibly reduced and oxidized between the Q and SQ oxidation states in MeCN in a 200 μL thin layer cell. UV/vis spectra were measured *in situ* upon reduction and oxidation by potential step measurements, and extinction coefficients were calculated for all absorption bands (Figure 3 and Table S1). Energies of excited states were calculated for identification of the observed transitions in the UV/vis spectra (Table S2). The energy diagram for **1** with the involved MOs is shown in Figure 4. In

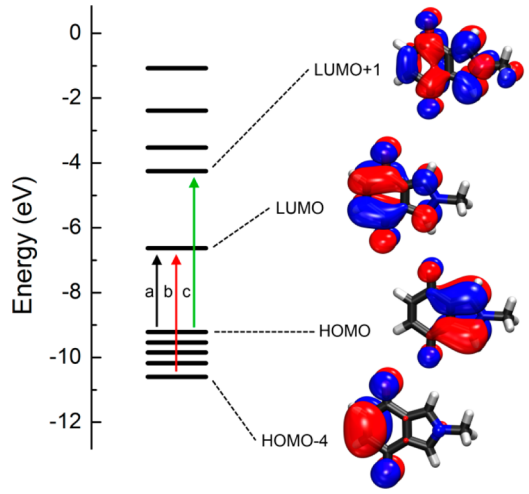

Figure 4. Energy diagram for **1** with the MOs involved in the major spectral transitions: (a) HOMO to LUMO, (b) HOMO−4 to LUMO, and (c) HOMO to LUMO+1.

the Q state, three absorption bands dominated the spectra: two transitions in the UV region and one transition with a tail in the visible region. Upon reduction several new absorption bands appeared, and a general red-shift of the spectra was observed. For **4** the relatively simple quinone spectrum was observed at potentials where both quinone units were in oxidized state, i.e., compound **5**.[20] The insets in Figure 1 show the variation of the absorbance at peak maximum for the absorption peak in the visible region as a function of applied potential during the quinone-to-semiquinone redox transition (red squares) and upon reoxidation (black circles).[21] The sigmoidal dependence of the absorbance with potential could be well represented by the expected Nernstian behavior for the redox reaction (solid lines), and the extracted reduction potential from the fit agreed within 16 mV with the data presented in Table 2. All spectral changes occurring in this potential interval showed the same behavior, indicating that all spectral features were in fact related to the Nernstian redox reaction. The reduction to the HQ state, on the other hand, was irreversible in the thin layer cell, and the potential at which the second reduction process was observed varied greatly, in contrast to the high reproducibility of the corresponding reaction in a bulk cell.[22]

3.3. Polymerization. Attempts to electropolymerize **1**−**4** were unsuccessful. Several conditions were tested, including different electrochemical techniques (potential steps or CV), substrates (glassy carbon, Pt, or Au), and solvents (MeCN or propylene carbonate, with or without addition of water). The monomers were oxidized to the cation radical species, but no polymer was formed under any conditions. Pyrrole or *N*-methylpyrrole formed polymers under the same conditions, albeit slightly overoxidized due to the high potentials needed to oxidize **1**−**4**. Copolymerization of **1**−**4** with either pyrrole or *N*-methylpyrrole was also attempted. A polymer film could indeed be formed, but there was no evidence of any incorporation of IID into the polypyrrole chain.

4. DISCUSSION

1 has previously been synthesized via a 3 + 2 cycloaddition of an azomethine ylide to *p*-benzoquinone.[7] **2**−**4** were synthesized here using the same procedure with substituted *p*-benzoquinones. The obtained yields were low (9−36%), but the reaction and purification conditions could probably be optimized to improve this, as the reaction has been performed in high yields (70−81%) with other substituted *p*-benzoquinones.[23,24] In the reaction starting from chloro-*p*-benzoquinone, both **1** and **2** were formed, with only a slight excess of **2**. The reaction thus works almost equally well with substitution of either Cl or H. It should therefore be possible to increase the yield of the desired product **2** using either 2,5-dichloro-*p*-benzoquinone or 2,6-dichloro-*p*-benzoquinone as the starting material. In our hands, the reaction does not proceed with chloranil (tetrachloro-*p*-benzoquinone) as the starting material, which would require substitution of two Cl atoms. The intended product 5,6-dichloro-2-methylisoindole-4,7-dione should instead be possible to synthesize using either 2,3-dichloro-*p*-benzoquinone or trichloro-*p*-benzoquinone as starting material in the reaction.

1−**4** were characterized by various electrochemical techniques in water and MeCN. In organic electrolyte, the redox system showed reversible behavior (reversibility diagnostics in Table 1) with two separate one-electron transfers that were diffusion controlled and allowed for calculation of diffusion coefficients. In general, diffusion coefficients were lower for the larger compounds, and also lower for the more reduced species, probably due to the stronger interaction of the hydroxy group with the solvent compared to the less polar quinone carbonyl group.

In aqueous electrolyte only one reduction peak was observed, which was irreversible, and cyclic voltammograms exhibited a much smaller oxidation peak compared to the reduction peak. The main difference between the aqueous and organic electrolytes is the availability of protons. The different oxidation states of IIDs (Q, SQ, and HQ) can be protonated once or twice depending on the acidic strength of the solvent (Scheme 2), e.g., for **3**: $pK_a(QH^{\bullet})$ = 12.8, $pK_a(QH_2^{\bullet+})$ = 6.2 (Pourbaix diagram in Figure 2). DFT calculations were therefore used to investigate which protonation states that are dominant.

A method based on DFT calculations was used previously to predict the electrochemical behavior of a series of IIDs, including those synthesized here.[7] A comparison of the experimentally determined redox potentials with those predicted from the computations are shown in Figure 5. The redox potentials of a few other compounds from the calculation series has also been determined previously,[25] namely 2,5-dimethylisoindole-4,7-dione (**6**, R = Me, R′ = H, see Scheme 1), 5-methoxy-2,6-dimethylisoindole-4,7-dione (**7**, R = OMe, R′ = Me), and 2-methylbenzo[*f*]isoindole-4,9-dione (**8**, R−R′ = −CH═CH−CH═CH−) and are included in Figure 5. The method has excellent predictive power, with a mean absolute

dx.doi.org/10.1021/jp311009z | J. Phys. Chem. C 2013, 117, 894−901

Scheme 2. Possible Protonation (Horizontal) and Redox (Vertical) Reactions of IIDs, Showing the Conversion between the Different Oxidation States (Q, SQ, and HQ) and Their Protonation Forms

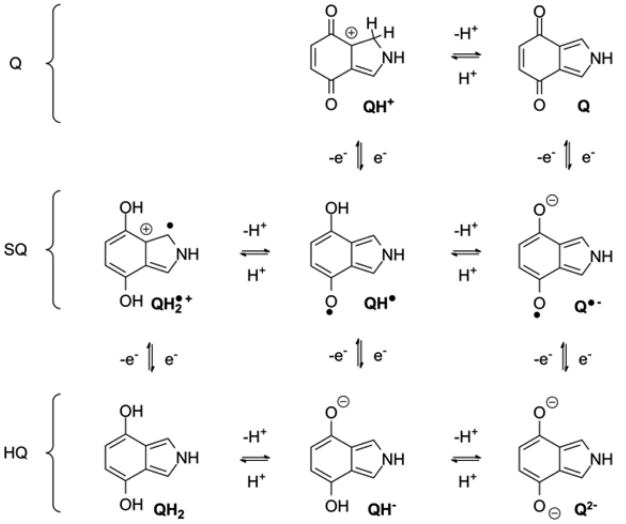

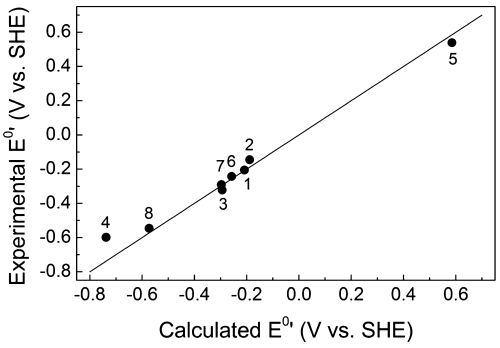

Figure 5. Comparison of calculated and experimental redox potentials in aqueous solution. The line is a guide for the eye representing equivalence (experimental = calculated).

deviation (MAD) of 38 mV, valid over almost the entire water potential window (−0.7 to +0.6 V vs SHE).

The largest discrepancy between experimental and calculated redox potentials is found for **4**, with a deviation of 139 mV, while the MAD for the rest of the series is only 24 mV. This error is probably related to the fact that interactions with specific solvent molecules are not accounted for in the calculations.[7] The computations predict that the HQ form of **4** will have two intramolecular hydrogen bonds. However, the free rotation around all C−O bonds allow for the possibility of hydrogen bonding with solvent molecules that will provide lower energy conformers. That will favor the reduction reaction and the predicted redox potential is thus too low. The Q form of **4** is also predicted to have two intramolecular hydrogen bonds. That conformer is probably the most stable one in solution, since there is no rotation around the C═O bonds.

DFT calculations were used to construct Pourbaix diagrams of **2**−**5** which were compared with the experimental results (Figure 2). In aqueous electrolyte buffered at pH = 7, **1**−**5** are reduced in one two-electron step, and the observed peak was thus assigned to the two-electron conversion from the Q to the HQ state. The reduction potential decreases with ∼59 meV/pH unit, showing that the reduction is proton coupled ($2e^-$, $2H^+$), going to the QH_2 species. This is in accordance with DFT calculations presented in a previous publication,[7] which predicted that the Q → QH_2 reduction would be preferred at neutral pH. At low pH (pH < 3 for **3**), the calculations predict that the Q → $QH_2^{\bullet+}$ reduction, which is a $1e^-$, $2H^+$ process, will be favored, resulting in a slope of −118 meV/pH. A stronger pH dependence of the reduction potential is indeed observed at low pH values for **1** and **3**, while this transition for the other compounds is at too low pH values to be observed here. The follow-up reaction $QH_2^{\bullet+}$ → QH_2 is not observed, indicating that the produced $QH_2^{\bullet+}$ radical is unstable in water. The same pattern is observed for all compounds in the series.

In nonprotic electrolyte, **1**−**4** are reduced in two one-electron steps, from the Q form to the HQ form via the SQ form. UV/vis spectra could be measured during electrochemical conversion between the Q and SQ forms (Figure 3). Figure 1 shows the visible absorbance for the reduction and reoxidation of the Q/SQ transition. Since the absorbance of all peaks follows the behavior expected from the Nernst equation and have identical inflection point unique for the respective compounds (Figure 1), all observed absorbance peaks were ascribed to the two investigated oxidation states of **1**−**4**. The Q form of **1**−**3** and **5** have three UV/vis absorbance bands, and DFT calculations were employed to identify the transitions. Energies obtained from DFT calculations of excited states correspond to the 0−0 transition, which is observed experimentally as the red edge of the bands. For all compounds in the Q form, the calculated transitions fit well with the observed spectra, and the three absorption bands could be assigned to specific transitions. The band at 369 nm in **1** has the lowest intensity and corresponds dominantly to the HOMO to LUMO transition. The band at 242 nm corresponds to the HOMO−4 to LUMO transition, and the band at 225 nm corresponds to the HOMO to LUMO+1 transition (energy diagram with MO plots in Figure 4). The dominant transitions observed in **2**, **3**, and **5** involve the same MOs as in **1**. None of the three protonation forms of SQ shows as good agreement between calculated and experimental spectra as for the Q form, but the best fit is obtained for $QH^{\bullet}$. Calculated transitions of $QH_2^{\bullet+}$ are also in reasonable agreement with experiments, while $Q^{\bullet-}$ completely fails to account for the lowest energy transition. It is concluded that the SQ form of **1**−**4** is protonated under these conditions, but it is uncertain if it is mono- or diprotonated. The more complicated spectrum of the SQ forms is likely due to the lost symmetry upon reduction. The existence of both an OH and an $O^{\bullet}$ group in the SQ species results in more possible energy levels that are approximately equal in energy. The same reasoning can explain the even more complicated spectrum of the Q form of **4**, which has both a Q and a HQ ring.

The positions of the two UV bands at shorter wavelengths do not vary greatly within the series of compounds (Figure 6). However, the energy of the visible transition shows a linear correlation with the reduction potential (r^2 = 0.99, Figure 6 and Table S1, including literature absorption data measured in MeOH[23,24]). This can be understood after examination of the MOs involved in the electronic transition (HOMO to LUMO, Figure 4). Since the electron density in LUMO is mainly located on the quinone moiety and the HOMO is located almost entirely on the pyrrole ring, this transition corresponds to a partial charge transfer transition between the pyrrole and the quinone. Substitution on the quinone ring, which is the difference between compounds **1**−**8**, will thus have a strong

dx.doi.org/10.1021/jp311009z | J. Phys. Chem. C 2013, 117, 894−901

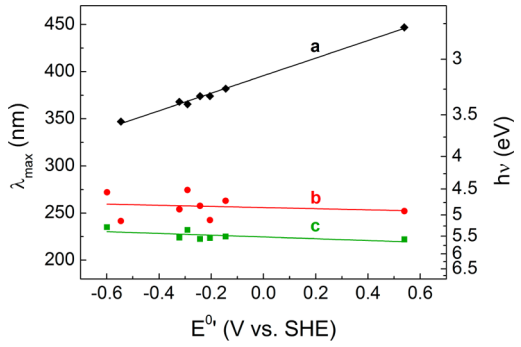

Figure 6. Location of absorbance maxima of transitions a−c in Figure 4 vs the reduction potential in aqueous solution. Lines show linear regressions (r^2 = 0.99 for a). Wavelength scale on the left *y*-axis and energy scale on the right *y*-axis. Values are shown in Table S1.

effect on the LUMO energy while leaving the HOMO energy relatively unaffected by substitution. The invariance in redox potential for the oxidation reaction in **1**−**5**, corresponding to the removal of an electron from the HOMO, gives further support for this idea. The transition energy (i.e., the energy difference between HOMO and LUMO) is therefore expected to vary linearly with the LUMO energy. The reduction potential of Q (Q/SQ, Table 2) corresponds to the energy required to add an extra electron in the LUMO. Since the HOMO energy is constant, the energy of the HOMO to LUMO absorption varies linearly with the reduction potential within the IID series (Figure 6).

The absorption at 240−280 nm shows no correlation between absorption maxima and substitution (reduction potential). Both the HOMO−4 and the LUMO are mainly located on the quinone ring, and the lack of correlation with substitution indicates that both MO energies are equally affected by substitution, which is reasonable since they are both quinone centered. The absorption at 220−240 nm corresponds to the HOMO to LUMO+1 transition. The LUMO+1 is distributed over the entire molecule, and this transition energy is expected to vary linearly with the LUMO+1 energy as, following the above reasoning, the HOMO energy is unaffected by substitution. There is, however, a modest decrease in absorption maximum with reduction potential. This suggests, somewhat surprisingly, that the HOMO is more strongly influenced by substitution than the LUMO+1 orbital or that the LUMO+1 energy has an inverse dependence of the substituents' electron-withdrawing power (Figure 6 and Table S1).

The pyrrole moiety of the IIDs provides a possibility for polymerization to form polypyrrole derivatives, which has already been applied to make polyisoindoles.[9] The possibility to polymerize **1**−**8** has previously been investigated theoretically.[7] Three conditions have to be fulfilled for successful oxidative polymerization of a pyrrole derivative: (i) the oxidation potential must be within the potential window of the solvent, (ii) the formed radical should be placed on carbons where dimerization occurs, and (iii) there should be sufficiently low steric hindrance at those positions to allow dimerization.[7] It was found that **1**−**8** meet the first requirement, but only **1**, **3**, **6**, and **8** meet the second requirement.[7] The third requirement, pertaining to accessibility of the reactive sites, is difficult to assess quantitatively.

In this study, none of the compounds **1**−**4** could be polymerized by electrochemical oxidation. The strain of an IID polymer is larger than for a polyisoindole due to the quinone oxygens. In **1**−**4** there is also a methyl group that would need to be situated close to an already crowded region of two oxygens. Steric hindrance is therefore a likely explanation for the lack of polymerization. Removal of the methyl group would decrease the strain while not affecting the redox chemistry of the molecule.[7] In principle, it should also be possible to copolymerize **1**−**4** with a less bulky monomer, such as pyrrole. However, pyrrole is much more easily oxidized than the IIDs and polymerizes quickly. Copolymerization attempts yielded no evidence of IID units incorporated into the polymer. A modification of this strategy would be to synthesize a less sterically hindered monomer, such as a pyrrole trimer with one unit being an IID (e.g., 1,3-dipyrrol-2-ylisoindole-4,7-dione). A completely different route toward polymerization would be to use some organometallic coupling reaction, starting from a dibrominated monomer.[26]

5. CONCLUSIONS

The electrochemistry of a series of IIDs was investigated and evaluated as a basis for organic polymer LIB cathodes. Three new IID derivatives, namely 5-chloro-2-methylisoindole-4,7-dione (**2**), 5-*tert*-butyl-2-methylisoindole-4,7-dione (**3**), and 5,8-dihydroxy-2-methylbenzo[*f*]isoindole-4,9-dione (**4**), were synthesized, demonstrating the versatility of the reaction. Spectroscopic and electrochemical characterization of the compounds was compared with results from a previously performed computational study, with very good agreement of redox potentials and acid dissociation constants.[7] The employed DFT strategy can hence be a valuable tool for understanding the complex redox chemistry of quinones, which is an important step in rational design of polymeric quinone LIB cathode materials. The one-electron redox reaction between Q and SQ could be followed spectroscopically *in situ*. The UV/vis transition of lowest energy had a high correlation with the redox potential, while the other two observed transitions had little or no dependence on the redox potential. This was discussed in terms of the electron distribution of the MOs involved in the transitions. Polymerization of the IIDs **1**−**5** could not be achieved electrochemically, but other routes toward IID polymers were discussed and will be explored further in future work. IIDs constitute a promising basis for LIB cathode materials, but the problems involved in polymerization need to be resolved.

■ ASSOCIATED CONTENT

Supporting Information

Complete ref 18, experimental and calculated UV/vis transitions, IR and NMR spectra. This material is available free of charge via the Internet at http://pubs.acs.org.

■ AUTHOR INFORMATION

Corresponding Author

*E-mail Martin.Sjodin@Angstrom.uu.se.

Author Contributions

The manuscript was written through contributions of all authors. All authors have given approval to the final version of the manuscript.

Notes

The authors declare no competing financial interest.

■ ACKNOWLEDGMENTS

The Swedish Research Council (VR), the Swedish Foundation for Strategic Research (SSF), the Swedish Energy Agency, the Swedish Centre for Smart Grids and Energy Storage (SweGRIDS), the European Institute of Innovation and Technology, under the KIC InnoEnergy Electric Energy Storage project, and the KIC InnoEnergy NewMat project as well as the Nordic Innovation Centre (contract number 10014) are acknowledged for their financial support.

■ ABBREVIATIONS

LIB, lithium ion battery; IID, isoindole-4,7-dione; DFT, density functional theory; TBAHFP, tetrabutylammonium hexafluorophosphate; SHE, standard hydrogen electrode; MO, molecular orbital; SWV, square wave voltammetry; DPV, differential pulse voltammetry; CV, cyclic voltammetry; Q, quinone; SQ, semiquinone; HQ, hydroquinone; MAD, mean absolute deviation.

■ REFERENCES

(1) Armand, M.; Tarascon, J.-M. *Nature* **2008**, *451* (7179), 652−657.
(2) Poizot, P.; Dolhem, F. *Energy Environ. Sci.* **2011**, *4* (6), 2003−2019.
(3) Liang, Y.; Tao, Z.; Chen, J. *Adv. Energy Mater.* **2012**, *2* (7), 742−769.
(4) Song, Z.; Zhan, H.; Zhou, Y. *Chem. Commun.* **2009**, *4*, 448−450.
(5) Chen, H.; Armand, M.; Courty, M.; Jiang, M.; Grey, C. P.; Dolhem, F.; Tarascon, J.-M.; Poizot, P. *J. Am. Chem. Soc.* **2009**, *131* (25), 8984−8988.
(6) Wang, C.; Appleby, A. J.; Little, F. E. *J. Electroanal. Chem.* **2002**, *519* (1−2), 9−17.
(7) Karlsson, C.; Jämstorp, E.; Strømme, M.; Sjödin, M. *J. Phys. Chem. C* **2012**, *116* (5), 3793−3801.
(8) Yoshida, H.; Uotani, N.; Saida, Y. In PCT Int. Appl., 1987.
(9) Rhee, S. B.; Lee, M.-H.; Moon, B. S.; Kang, Y. *Korea Polym. J.* **1993**, *1* (1), 61−68.
(10) Han, X.; Chang, C.; Yuan, L.; Sun, T.; Sun, J. *Adv. Mater.* **2007**, *19* (12), 1616−1621.
(11) Olsson, H.; Nyström, G.; Strømme, M.; Sjödin, M.; Nyholm, L. *Electrochem. Commun.* **2011**, *13* (8), 869−871.
(12) Naegele, D.; Bittihn, R. *Solid State Ionics* **1988**, *28*−*30* (Part 2), 983−989.
(13) Chambers, J. Q. In *The Chemistry of the Quinonoid Compounds*; Patai, S., Ed.; John Wiley & Sons: London, 1974; Vol. *1*, pp 737−791.
(14) Shim, Y.-B.; Park, S.-M. *J. Electroanal. Chem.* **1997**, *425* (1−2), 201−207.
(15) Cape, J. L.; Bowman, M. K.; Kramer, D. M. *Phytochemistry* **2006**, *67* (16), 1781−1788.
(16) Namazian, M.; Almodarresieh, H. A.; Noorbala, M. R.; Zare, H. R. *Chem. Phys. Lett.* **2004**, *396* (4−6), 424−428.
(17) Lao, K.-U.; Yu, C.-H. *J. Comput. Chem.* **2011**, *32* (12), 2716−2726.
(18) Frisch, M. J.; Trucks, G. W.; Schlegel, H. B.; Scuseria, G. E.; Robb, M. A.; Cheeseman, J. R.; Scalmani, G.; Barone, V.; Mennucci, B.; Petersson, G. A.; et al. *Gaussian 09*; Gaussian Inc.: Wallingford, CT, 2009.
(19) Humphrey, W.; Dalke, A.; Schulten, K. *J. Mol. Graphics* **1996**, *14* (1), 33−38.
(20) Note that this redox reaction might involve adsorption of **5** to the electrode, and therefore the concentration and the evaluated extinction coefficients for **5** are uncertain.
(21) Reduction to the hydroquinone form of **4** is also shown in Figure 1d, but reoxidation is not shown due to poor reversibility.
(22) The large variations in water content in organic solvents and the ability to accommodate or provide protons make it difficult to control the protonation level of an analyte. The poor reproducibility and reversibility of the second reduction (SQ/HQ) in a thin layer cell is ascribed to variations in the concentration of water or oxygen.
(23) Schubert-Zsilavecz, M.; Schramm, H. W. *Liebigs Ann. Chem.* **1991**, *9*, 973.
(24) Schubert-Zsilavecz, M.; Likussar, W.; Gusterhuber, D.; Michelitsch, A. *Monatsh. Chem.* **1991**, *122* (5), 383−387.
(25) Schubert-Zsilavecz, M.; Michelitsch, A.; Likussar, W. *Monatsh. Chem.* **1992**, *123* (12), 1223−1225.
(26) Yamamoto, T.; Saito, N. *Macromol. Chem. Phys.* **1996**, *197* (1), 165−175.
(27) Also contains a contamination of **1**.